energies

MDPI

Article

An Improved Continuous-Time Model Predictive Control of Permanent Magnetic Synchronous Motors for a Wide-Speed Range

Dandan Su [1,2], Chengning Zhang [1,2,*] and Yugang Dong [1,2]

[1] National Engineering Laboratory for Electric Vehicles, Beijing Institute of Technology, Beijing 100081, China; 3120130176@bit.edu.cn (D.S.); dygmjily@163.com (Y.D.)

[2] Collaborative Innovation Center of Electric Vehicle in Beijing, 5 South Zhongguancun Street, Haidian District, Beijing 100081, China

* Correspondence: mrzhchn@bit.edu.cn; Tel.: +86-(10)-6891-4842

Received: 26 October 2017; Accepted: 30 November 2017; Published: 4 December 2017

Abstract: This paper proposes an improved continuous-time model predictive control (CTMPC) of permanent magnetic synchronous motors (PMSMs) for a wide-speed range, including the constant torque region and the flux-weakening (FW) region. In the constant torque region, the mathematic models of PMSMs in dq-axes are decoupled without the limitation of DC-link voltage. However, in the FW region, the mathematic models of PMSMs in dq-axes are cross-coupled together with the limitation of DC-link voltage. A nonlinear PMSMs mathematic model in the FW region is presented based on the voltage angle. The solving of the nonlinear mathematic model of PMSMs in FW region will lead to heavy computation load for digital signal processing (DSP). To overcome such a problem, a linearization method of the voltage angle is also proposed to reduce the computation load. The selection of transiting points between the constant torque region and FW regions is researched to improve the performance of the driven system. Compared with the proportional integral (PI) controller, the proposed CTMPC has obvious advantages in dealing with systems' nonlinear constraints and improving system performance by restraining overshoot current under step torque changing. Both simulation and experimental results confirm the effectiveness of the proposed method in achieving good steady-state performance and smooth switching between the constant torque and FW regions.

Keywords: permanent magnetic synchronous motors; continuous-time model predictive control; flux-weakening; smooth transition

1. Introduction

Nowadays, permanent magnetic synchronous motors (PMSMs) have been widely applied in electric vehicle, train, electric aircraft, and so on, due to high efficiency and high torque/ampere ratio [1,2]. Many control algorithms for PMSMs have been widely researched and successfully applied to a wide range of drive applications [3].

The proportional integral (PI) controller is a traditional control algorithm that has been widely applied in industry. Since the control system of PMSMs is a nonlinear system with unavoidable disturbances and parameter variations, it is difficult for the PI controller to obtain a satisfying dynamic performance in the entire operating range [4]. A lot of intelligence control algorithms are also proposed, such as sliding mode control [5,6], adaptive control [7,8], neural network control [9,10], and so on. However, their dependence on the motor parameters and heavy computation load limit their application on PMSMs.

Recently, model-based predictive control (MPC) strategies have received attention in research communities due to their faster dynamic response, precise steady-state performance, easy implementation, and easy inclusion of nonlinearities and constraints [11–13]. MPC can be classified into two types: the finite set MPC (FSMPC) and the continuous-time MPC (CTMPC) [14].

FSMPC exploits the inherent discrete nature of power converters, does not require a modulator, has an intuitive concept, and is easy to understand. Among all available FSMPC in power electronics, predictive current control (PCC) and predictive torque control (PTC) are two most popular control methods [15].

There are main challenges of the PCC in industrial deployment, such as the uncertainty of model parameters [16,17], measurement noise [18], and varying switching frequency [19]. Ref. [20] analyzed the parameter sensitivity of PCC and adopted a disturbance observer (SCDO) to track the disturbance caused by parameter mismatch. PCC with Kalman filtering and inductance profile auto-calibration was presented in [21], which aimed to improve the performance of switched reluctance motors (SRMs) current control. To achieve a constant switching frequency and improve transient characteristics under faster speed changing, the proposed controller in [22] combined deadbeat control and PCC techniques. However, the complexity of the controller was increased. PTC was proposed recently as an effective control scheme in the application of high performance torque control of motor drives. The vector selection of PTC is more effective than conventional direct torque control (DTC), which uses a switching table [23,24]. The cost function of PTC usually consists of torque and flux magnitude errors, which are different in unit and magnitude, where a proper weighting factor is required to achieve satisfactory performance [25]. To reduce the torque ripple of PTC, an improved PTC applied in an inductance motor (IM) was proposed based on the inherent relationship between the stator current and stator flux [26]. A simplified PTC was presented in [27] based on a new switching table, where both the number of prediction vectors and the computational load were reduced by considering the position of stator flux and the sign of torque deviation.

CTMPC is one of the most popular formulations among the MPC algorithms, and has been successfully implemented in industry [28]. CTMPC only considers the past and present tracking errors and can ensure the near-optimal performance of the system by minimizing a cost function. Moreover, CTMPC requires a pulse-width modulation (PWM) modulator, but it is designed to deal, especially, with non-linear systems having fast dynamics [29]. A novel CTMPC approach was proposed in [30] for the control of sensorless induction motors (IMs). The multivariable CTMPC controller allowed the rotor flux and speed tracking simultaneously while considering constraints of voltage and current. In [31], a nonlinear CTMPC for IMs had been developed. It included system state variables of stator currents, as well as rotor flux and speed. The rotor speed, flux and the load torque were estimated using an extended Kalman filter (EKF). A CTMPC of PMSMs with disturbance decoupling was proposed in [32]. The predicted speed tracking error was directly used to determine the required voltage command without the need of a cascaded control scheme. Ref. [33] presented a robust continuous nonlinear model predictive control (CNMPC) for a grid-connected photovoltaic (PV) inverter system. The objective of the proposed approach was to control the power exchange between the grid and the PV system, while achieving unity power factor operation.

This paper proposed an improved CTMPC of PMSMs for a wide-speed range including the constant torque region and flux-weakening (FW) region. In the constant torque region, a linear mathematic model of PMSMs is presented to predict dq-axes voltages. In the FW region, since dq-axes voltages are coupled together due to the limitation of DC-link voltage, a nonlinear mathematic model of CTMPC of PMSMs based on the voltage angle control is proposed. Since solving the complicated mathematical model of PMSMs in the FW region will cost a lot of time, the increment of voltage angle is linearized at each sample instant to predict the system future dynamics and reduce computation load for digital signal processing (DSP). The smooth transitions between the constant torque region and the FW region are also considered and presented in this paper.

This paper is organized as follows: The principle of CTMPC is analyzed in Section 2. In Section 3, the proposed improved CTMPC is shown; this section is divided into three parts: CTMPC in the constant torque region, CTMPC in the FW region, and the smooth transition between them. The simulation and experiment results are presented in Section 4. This paper is concluded with a summary in Section 5.

2. Continuous-Time Model Predictive Control

The predictive algorithm of CTMPC involves a class of control techniques, which utilize a process model to predict the system future behavior, with the control law obtained by optimizing a cost function that considers the following: (1) the effort necessary for control, and (2) the difference between predicted output values and reference values. In order to apply the first element of the optimal sequence, a receding-horizon principle is adopted. Since the future behavior of the system needs to be predicted, the model of the system is the core of CTMPC. A discrete-time state-space model is considered as the follows:

$$x(k+1) = Ax(k) + B_u u(k) + B_d d(k) \tag{1}$$

$$y_c(k) = C_c x(k) \tag{2}$$

where $x(k) \in \mathbb{R}^{n_x}$ is the state variable, $u(k) \in \mathbb{R}^{n_u}$ is the input variable, $y_c(k) \in \mathbb{R}^{n_c}$ is the output variable, and $d(k) \in \mathbb{R}^{n_d}$ is the disturbance from outside which can be measured. A, B_u, B_d, and C_c are the coefficients of variables respectively.

To reduce the steady-state error of the output, the prediction is derived by Equations (3) and (4) with an incremental model.

$$\Delta x(k+1) = A\Delta x(k) + B_u \Delta u(k) + B_d \Delta d(k) \tag{3}$$

$$y_c(k) = C_c \Delta x(k) + y_c(k-1) \tag{4}$$

where

$\Delta x(k) = x(k) - x(k-1);$
$\Delta u(k) = u(k) - u(k-1);$
$\Delta d(k) = d(k) - d(k-1).$

The predicted output of system is given by (5)

$$y_c(k+1|k) = A\Delta x(k) + C_c y_c(k) + B_u \Delta u(k) + B_b \Delta d(k) \tag{5}$$

where $y_c(k + 1 \mid k)$ is the predicted output at instant $k + 1$ based on the output at instant k.

To make sure the predicted output is close to the reference output, the following cost function is adopted.

$$J = \|\mathit{\Gamma}_y y_c(k+1|k) - r_j(k+1)\|^2 + \|\mathit{\Gamma}_u \Delta u(k)\|^2 \tag{6}$$

where $\mathit{\Gamma}_y$ and $\mathit{\Gamma}_u$ are weight coefficients. $\mathit{\Gamma}_y$ is a defined positive variable, allowing an emphasis on each of the controlled outputs and its predictions. $\mathit{\Gamma}_u$ is a defined positive variable, which weights the control efforts of inputs. r_j $(k + 1)$ is the reference output variable.

A new variable is defined as follows in order to obtain the minimum value of cost function.

$$
\begin{aligned}
\rho &\overset{\text{def}}{=} \begin{bmatrix} \Gamma_y(y_c(k+1|k) - r(k+1)) \\ \Gamma_u \Delta u(k) \end{bmatrix} \\
&= \begin{bmatrix} \Gamma_y B_u \\ \Gamma_u \end{bmatrix} \Delta u(k) - \begin{bmatrix} \Gamma_y \overbrace{(r(k+1) - A\Delta x(k) - B_u y_c(k) - B_d \Delta d(k))}^{E_p(k+1|k)} \\ 0 \end{bmatrix} \\
&= \underbrace{\begin{bmatrix} \Gamma_y B_u \\ \Gamma_u \end{bmatrix} \Delta u(k)}_{Sz} - \underbrace{\begin{bmatrix} \Gamma_y E_p(k+1|k) \\ 0 \end{bmatrix}}_{b} \\
&= Sz - b
\end{aligned} \tag{7}
$$

where

$$z = \Delta u(k) \quad S = \begin{bmatrix} \Gamma_y B_u \\ \Gamma_u \end{bmatrix} \quad b = \begin{bmatrix} \Gamma_y E_p(k+1|k) \\ 0 \end{bmatrix};$$

$$E_p(k+1|k) = r(k+1) - A\Delta x(k) - C_c y_c(k) - B_d \Delta d(k).$$

Then, the cost function can be rewritten as follows:

$$J = \rho^{\mathrm{T}} \rho \tag{8}$$

The minimum value of cost function can be calculated by:

$$\frac{d\rho^{\mathrm{T}}\rho}{dz} = 2\left(\frac{d\rho}{dz}\right)^{\mathrm{T}} \rho = 2S^{\mathrm{T}}(Sz - b) = 0 \tag{9}$$

Since the second derivation of (8) is bigger than zero (Equation (10)), the extreme value of cost function is the minimum value.

$$\frac{d^2(\rho^{\mathrm{T}}\rho)}{dz^2} = 2S^{\mathrm{T}}S > 0 \tag{10}$$

The minimum value of cost function is:

$$
\begin{aligned}
z^* &= \left(S^{\mathrm{T}}S\right)^{-1} S^{\mathrm{T}} b \\
&= \left(B_u^{\mathrm{T}} \Gamma_y^{\mathrm{T}} \Gamma_y B_u + \Gamma_u^{\mathrm{T}} \Gamma_u\right)^{-1} B_u^{\mathrm{T}} \Gamma_y^{\mathrm{T}} \Gamma_y E_p(k+1|k)
\end{aligned} \tag{11}
$$

The optimal incremental input at instant k is

$$\Delta u^*(k) = K_{\text{mpc}} E_p(k+1|k) \tag{12}$$

$$K_{\text{mpc}} = \left(B_u^{\mathrm{T}} \Gamma_y^{\mathrm{T}} \Gamma_y B_u + \Gamma_u^{\mathrm{T}} \Gamma_u\right)^{-1} B_u^{\mathrm{T}} \Gamma_y^{\mathrm{T}} \Gamma_y \tag{13}$$

where $\Delta u^*(k)$ is the optimal incremental input at instant k.

Constraints are inevitable in system, such as the extreme values, increment of control variables, and so on. Usually, these constraints are presented as follows:

$$\begin{cases} y_{\min} \le y_c \le y_{\max} & \forall k \ge 0 \\ u_{\min} \le u^* \le u_{\max} & \forall k \ge 0 \\ \Delta u_{\min} \le \Delta u^* \le \Delta u_{\max} & \forall k \ge 0 \end{cases} \tag{14}$$

where $y_{\min}(k)$ and $y_{\max}(k)$ are the minimum and maximum values of output variable, respectively, $u_{\min}(k)$ and $u_{\max}(k)$ are the minimum and maximum values of input variable, respectively, and $\Delta u_{\min}(k)$ and $\Delta u_{\max}(k)$ are the minimum and maximum incremental values of input variable, respectively.

3. Improved CTMPC of PMSMs for a Wide-Speed Range

Improved CTMPC control algorithms of PMSMs are proposed in this paper. The block diagram of the proposed control system is shown in Figure 1. The proposed algorithms can be applied for a wide-speed range including the constant torque region and the FW region. In the constant torque region, one CTMPC control algorithm is proposed based on the maximum torque per ampere (MTPA) control to increase system efficiency. In the FW region, another CTMPC is proposed according to the nonlinear property of PMSMs driven system. The detailed introduction of the control diagram will be elaborated in the following text.

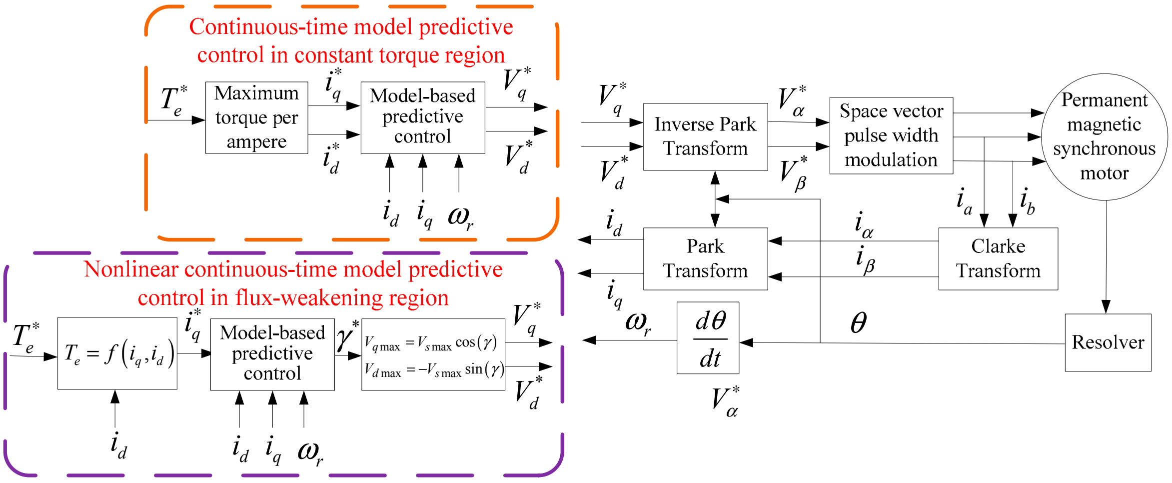

Figure 1. Block diagram of the proposed control system for a wide-speed range.

3.1. CTMPC of PMSMs in the Constant Torque Region

The mathematical model of PMSMs drive system can be described by the following equations in synchronous rotating dq reference frame:

$$\begin{aligned} v_q &= R_s i_q + L_q \frac{di_q}{dt} + \omega_r L_d i_d + \omega_r \lambda_f \\ v_d &= R_s i_d + L_d \frac{di_d}{dt} - \omega_r L_q i_q \\ v_s &= \sqrt{v_q^2 + v_d^2} \qquad\qquad v_s < v_{s\max} \end{aligned} \tag{15}$$

where

R_s: Stator winding resistance;
i_d, i_q: d and q axes currents;
v_d, v_q: d and q axes voltages;
L_d, L_q: d and q axes inductances;
ω_r: Electrical speed in rad/sec;
λ_f: Magnet flux linkage;
v_s: The output voltage of inverter;
$v_{s\max}$: The maximum output voltage of inverter limited by the DC-link voltage.

In the constant torque region, the output voltag e (v_s) of the inverter is smaller than the maximum output voltage of the inverter ($v_{s\max}$). Without the DC-link voltage limitations, the PMSMs mathematical model is a linear equation group. The relationship of dq-axes voltages (v_d, v_q) can be decoupled. Due to the decoupling relationship of v_d and v_q, the solutions of i_d and i_q will be many groups when the reference torque and speed are given. The i_d and i_q, which can minimize the system currents, will be adopted to increase system efficiency called MTPA control.

In DSP, the continuous-time representation of system model has to be transformed into a discrete-time representation based on the forward Euler approximation with a sampling period T_s.

$$\frac{dx}{dt} \approx \frac{x(k+1) - x(k)}{T_s} \tag{16}$$

where T_s is a constant sampling time substituting for dt.

With the transformations of (16), the discrete-time PMSMs model can be obtained as follows

$$\begin{bmatrix} i_q(k+1) \\ i_d(k+1) \end{bmatrix} = A_{\mathrm{MTPA}} \begin{bmatrix} i_q(k) \\ i_d(k) \end{bmatrix} + B_{u\mathrm{MTPA}} \begin{bmatrix} v_q(k) \\ v_d(k) \end{bmatrix} + B_{d\mathrm{MTPA}} \omega_r(k) \tag{17}$$

$$y_c(k) = C_c \begin{bmatrix} i_q(k+1) \\ i_d(k+1) \end{bmatrix} \tag{18}$$

where $A_{\mathrm{MTPA}} = \begin{bmatrix} -\frac{R_s T_s}{L_d} + 1 & 0 \\ 0 & -\frac{R_s T_s}{L_q} + 1 \end{bmatrix}$ $B_{u\mathrm{MTPA}} = \begin{bmatrix} \frac{T_s}{L_d} & 0 \\ 0 & \frac{T_s}{L_q} \end{bmatrix}$ $B_{d\mathrm{MTPA}} = \begin{bmatrix} -\frac{L_d}{L_q} T_s i_d(k) & -\lambda_f \frac{T_s}{L_q} \\ \frac{L_q}{L_d} T_s i_q(k) & 0 \end{bmatrix}$ $C_c = \begin{bmatrix} 1 \\ 1 \end{bmatrix}$.

In the discrete-time PMSMs model, $i_d(k)$ and $i_q(k)$ are considered as the state variables and the output variables simultaneously. $v_d(k)$ and $v_q(k)$ are considered as the input variables. $\omega_r(k)$ is considered to be an external disturbance which can be measured.

To reduce the steady-state error of the dq-axes currents, an incremental model of PMSMs is applied as follows.

$$\begin{bmatrix} \Delta i_q(k+1) \\ \Delta i_d(k+1) \end{bmatrix} = A_{\mathrm{MTPA}} \begin{bmatrix} \Delta i_q(k) \\ \Delta i_d(k) \end{bmatrix} + B_{u\mathrm{MTPA}} \begin{bmatrix} \Delta v_q(k) \\ \Delta v_d(k) \end{bmatrix} + B_{d\mathrm{MTPA}} \Delta\omega_r(k) \tag{19}$$

$$y_c(k) = C_c \begin{bmatrix} \Delta i_q(k+1) \\ \Delta i_d(k+1) \end{bmatrix} + y_c(k-1) \tag{20}$$

Equation (21) is the cost function of CTMPC which means that the actual dq-axes currents are changing close to the reference values.

$$J = \begin{bmatrix} \| i_q(k+1|k) - i_q^*(k+1) \| \\ \| i_d(k+1|k) - i_d^*(k+1) \| \end{bmatrix} \tag{21}$$

where $i_q(k + 1 | k)$ and $i_d(k + 1 | k)$ are the predicted dq-axes currents at instant $k + 1$ based on dq-axes currents at instant k; $i^*_q(k + 1)$ and $i^*_d(k + 1)$ are the reference dq-axes currents at instant $k + 1$.

By the minimization of the cost function (21), the optimal increment of input voltages at instant k can be obtained by (22) based on (12) in numerical method.

$$\Delta u^*(k) = \begin{bmatrix} \Delta v_q^*(k) \\ \Delta v_d^*(k) \end{bmatrix} \tag{22}$$

where $\Delta v^*_q(k)$ and $\Delta v^*_d(k)$ are the optimal incremental dq-axs voltages at instant k.

To limit the extreme values and the increment of the input voltages, the following constraints are applied in the CTMPC.

$$\begin{cases} -v_{\text{smax}} \leq v_q^* \leq v_{\text{smax}} \\ -v_{\text{smax}} \leq v_d^* \leq v_{\text{smax}} \\ -\Delta v_{q\text{max}} \leq \Delta v_q^* \leq \Delta v_{q\text{max}} \\ -\Delta v_{d\text{max}} \leq \Delta v_d^* \leq \Delta v_{d\text{max}} \end{cases} \tag{23}$$

where Δv_{qmax} and Δv_{dmax} are the maximum incremental values of dq-axes voltages.

3.2. CTMPC of PMSMs Based on Voltage Angle Control in the Flux-Weakening Region

In the FW region, the maximum output voltage (v_{smax}) of the inverter is limited by DC-link voltage (V_{DC}). According to the location of v_{smax} in the hexagon of the stationary αβ frame, v_{smax} varies from $V_{dc}/\sqrt{3}$ to $2V_{DC}/3$ shown in Figure 2a. In this paper, v_{smax} is set to $\text{V}_{dc}/\sqrt{3}$ to increase the DC-link voltage utilization level and reduce torque ripple. Figure 2b shows the vector diagram of PMSMs in the synchronously rotating frame in the FW region, and γ is the angle between v_{smax} and v_q which is called the voltage angle. Since v_{smax} is set to a constant value, v_d and v_q can be represented by:

$$\begin{aligned} v_q &= v_{\text{smax}} \cos\gamma \\ v_d &= -v_{\text{smax}} \sin\gamma \end{aligned} \tag{24}$$

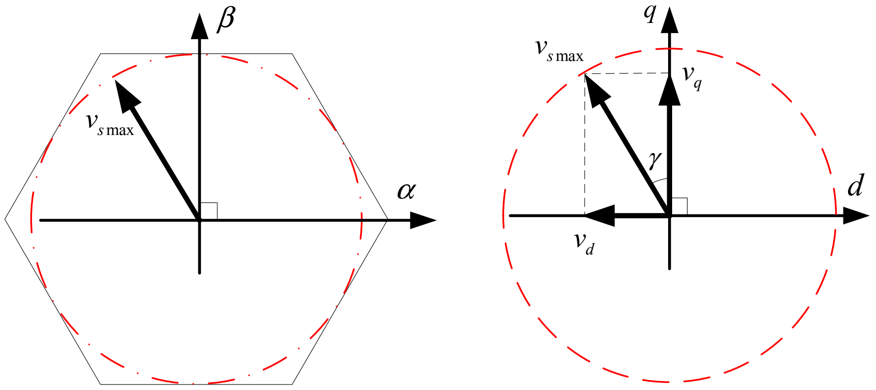

(**a**) (**b**)

Figure 2. The vector diagram of permanent magnetic synchronous motors in the flux-weakening region. (**a**) The voltage hexagon in the stationary αβ frame; (**b**) The vector diagram in the synchronously rotating frame.

Consequently, the key of FW control is how to obtain γ with the restrain of v_{smax}. The PMSMs model in the FW region can be rewritten as:

$$\frac{d}{dt}\begin{bmatrix} i_q \\ i_d \end{bmatrix} = \begin{bmatrix} \frac{1}{L_q} & 0 \\ 0 & \frac{1}{L_d} \end{bmatrix}\begin{bmatrix} v_{\text{smax}}\cos\gamma \\ -v_{\text{smax}}\sin\gamma \end{bmatrix} + \begin{bmatrix} -\frac{R_s}{L_q} & 0 \\ 0 & -\frac{R_s}{L_d} \end{bmatrix}\begin{bmatrix} i_q \\ i_d \end{bmatrix} + \begin{bmatrix} -\frac{L_d i_d}{L_q} & -\frac{\lambda_f}{L_q} \\ \frac{L_q i_q}{L_d} & 0 \end{bmatrix}\omega_r \tag{25}$$

In the FW region, v_d and v_q are cross-coupled together by the limitation of the DC-link output voltage shown in (24). The mathematical model of PMSMs is changing to a single-input and multiple-output (SIMO) system in the FW region. When *dq* reference currents (i^{*}_{d} and i^{*}_{q}) are given, γ can be calculated according to (25) since v_{smax} has been set to a constant value. Therefore, there is only one pair solution of v_d and v_q. The solution of v_d and v_q can be obtained by adjusting γ through q-axis voltage equation.

The q-axis discrete-time PMSMs model in the FW region can be rewritten as:

$$i_q(k+1) = A_{\text{FW}} i_q(k) + B_{u\text{FW}} \sin\gamma(k) + B_{d\text{FW}}\omega_r(k) \tag{26}$$

where $A_{\mathrm{FW}} = -R_s T_s / L_q + 1$, $B_{u\mathrm{FW}} = v_{s\max}$, $B_{d\mathrm{FW}} = -\left(L_d T_s i_d(k)/L_q + \lambda_f T_s / L_q\right) * (P/2)$, and P is the number of poles.

In the q-axis PMSMs model of (26), i_q is considered as the state variable and the output variable at the same time, i_d is one of coefficient in $B_{d\mathrm{FW}}$, while γ is considered as the input variables, and ω_r is considered to be the external disturbance which can be measured.

To solve such a complicated nonlinear equation group on line may cause heaven computation load for DSP. Therefore, the increment of voltage angle $\Delta\gamma$ is linearized at each sample instant in this paper.

The increment of v_q at instant k can be calculated based on trigonometric function as:

$$\begin{aligned} \Delta v_q(k) &= v_q(k+1) - v_q(k) \\ &= v_{s\max}(\cos(\gamma(k+1)) - \cos(\gamma(k))) \\ &= -2v_{s\max} \sin\tfrac{\gamma(k+1)+\gamma(k)}{2} \sin\tfrac{\gamma(k+1)-\gamma(k)}{2} \end{aligned} \tag{27}$$

Assuming $\Delta\gamma(k) = \gamma(k) - \gamma(k-1)$, because the sampling time T_s is very small that:

$$\begin{aligned} \sin\tfrac{\gamma(k+1)-\gamma(k)}{2} &\approx \tfrac{\Delta\gamma(k)}{2} \\ \tfrac{\gamma(k+1)+\gamma(k)}{2} &\approx \gamma(k) \end{aligned} \tag{28}$$

where $\Delta\gamma(k)$ is the increment of voltage angle at instant k.

The increment of v_q can be rewritten as:

$$\Delta v_q(k) = -v_{s\max} \sin\gamma(k) \Delta\gamma(k) \tag{29}$$

So far, the control variable $\Delta v_q{}^*(k)$ can be replaced by $\Delta\gamma^*(k)$ in (26). The voltage angle control can be applied as follows.

$$\Delta\gamma^*(k) = -\frac{1}{v_{s\max}\sin\gamma(k)} \Delta v_q^*(k) \tag{30}$$

where $\Delta\gamma^*(k)$ is the reference increment of voltage angle $\gamma(k)$ at instant k.

The incremental model of PMSMs in the FW region is shown as:

$$\Delta i_q(k+1) = A_{\mathrm{FW}} \Delta i_q(k) + B_{u\mathrm{FW}} \sin\gamma(k) \Delta\gamma(k) + B_{d\mathrm{FW}} \Delta\omega_r(k) \tag{31}$$

The following constrains of γ are applied to limit the extreme value and increment.

$$\begin{cases} 0 \le \gamma \le pi/2 \\ -\Delta\gamma_{\max} \le \Delta\gamma \le \Delta\gamma_{\max} \end{cases} \tag{32}$$

where $\Delta\gamma_{\max}$ is the maximum increment of voltage angle γ.

In the FW region, the reference current $i_q{}^*$ of PMSMs can be calculated by the reference torque $T_e{}^*$ and i_d shown in (33):

$$i_q^* = \frac{T_e^*}{\frac{3}{2}\frac{P}{2}\left(\left(L_d - L_q\right) i_d + \lambda_f\right)} \tag{33}$$

The cost function (34) means i_q is changing close to the reference value.

$$J = {}_{i=1}^{p} \left\| i_q(k+i|k) - i_q^*(k+i) \right\|^2 \tag{34}$$

By the minimization of the cost function (30), the optimal incremental voltage angle of driven system at instant k can be obtained by (34) based on (12).

$$\Delta u^*(k) = \Delta\gamma^*(k) \tag{35}$$

3.3. Smooth Transition of CTMPC between the Constant Torque Region and the FW Region

Since different CTMPC methods are adopted in the constant torque region and the FW region, the smooth transitions are also studied in this paper.

The smooth transition between the constant torque and the FW regions is primarily to ensure that the actual value of torque is basically the same as the reference value. Two questions about the transition are proposed in this paper. The first one is how to find the point where the constant torque region must switch to the FW region, and the second one is how to find the point where the FW region should change back to the constant torque region. Figure 3 shows the transitions between the constant torque and FW regions. When motors are working in the constant torque region, the modulation index (MI) should be calculated. If MI is smaller than 0.907, the motor will remain working in the constant torque region, and when MI is equal or bigger than 0.907, the motor should work in the FW region. When the motor works in the FW region, the d-axis current is used as the switching condition since MI is equal to 0.907 during the FW region.

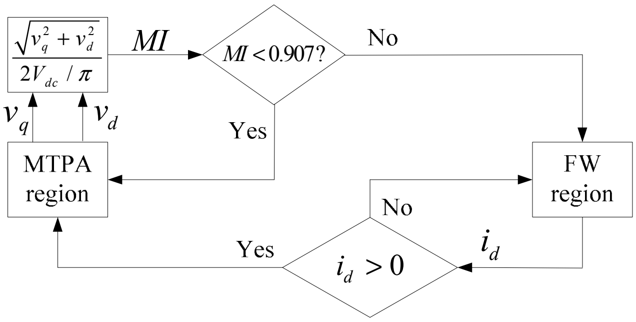

Figure 3. The transition between the constant torque and the flux-weakening regions.

3.3.1. The Constant Torque Region Transiting to the FW Region

At the point where the constant torque region should change to the FW region, according to (15), i_q, i_d, and ω_r are three important state variables in the transiting point selection. Besides these, the DC-link voltage, MI, parameters of driven system (such as resistance, inductance), and the nonlinearity of the inverter can also influence the selection of transiting point. Consequently, the selection of transiting point under changing parameters is difficult.

In this paper, the maximum value of MI is set to 0.907 to balance the utilization level of DC-link voltage and the torque ripple minimization. Therefore, when the MI reaches 0.907 the constant torque region must change to the FW region. MI can be calculated by (36).

$$\mathrm{MI} = \frac{v_s}{2V_{dc}/\pi} \tag{36}$$

After the transiting point is determined, the initial value of γ_0 has to be calculated. If γ_0 is chosen improperly, the output torque will deviate from the reference value. Consequently, the initial value of γ_0 is another important problem to ensure the smooth transition. The relationship between d-q axes voltage and γ_0 is (37), since both of the constant torque control and the FW control algorithms are applicable at the transiting point.

$$\begin{cases} v_{q0} = v_{\mathrm{smax}} \cos \gamma_0 \\ v_{d0} = -v_{\mathrm{smax}} \sin \gamma_0 \end{cases} \tag{37}$$

where v_{d0}, v_{q0} are d-q axes voltages at the transiting point.

The initial value of voltage angle γ_0 can be calculated by:

$$\gamma_0 = \arg\cos\left(\frac{v_{q0}}{v_{\mathrm{smax}}}\right) \tag{38}$$

3.3.2. The FW Region Changes Back to the Constant Torque Region

Due to the decreasing of reference speed/torque or the rising of DC-link voltage, FW region should change back to the constant torque region. Since MI is a control parameter, it is impossible to determine the transiting point based on MI. Now, we will analyze the influence on dq-axes currents if adopting FW control algorithm on the constant torque region under the same reference torque and speed.

In the constant torque region with the same reference torque and speed, if the FW control algorithm is adopted, the value of v_s will be $v_{s\max}$ which is bigger than required. Under this circumstance, the currents under the FW control algorithm will be bigger than the constant torque control algorithm according to (15), shown as follows.

$$i_{q\_\mathrm{MTPA}}^2 + i_{d\_\mathrm{MTPA}}^2 < i_{q\_\mathrm{FW}}^2 + i_{d\_\mathrm{FW}}^2 \tag{39}$$

where i_{q_MTPA} and i_{d_MTPA} are dq-axis currents in constant torque region when the MTPA control algorithm is adopted, i_{q_FW} and i_{d_FW} are dq-axis currents in constant torque region when the FW control algorithm is adopted.

For surface mounted PMSMs (SMPMSM), the q-axis current will not change under the same output torque regardless what control algorithm is adopted since the d-axis current cannot produce torque. Therefore the higher part of currents will be d-axis current. Consequently, the transiting point where the FW region should return back to the constant torque region is when i_d is bigger than zero. For interior PMSMs (IPMSMs), the d-axis current can produce reluctance torque because L_q is bigger than L_d. However, the q-axis current has the main contribution to output torque contrasting with reluctance torque. The higher part of current will also be d-axis current when FW control algorithm is adopt in the constant torque region. The transiting point where the FW region should return back to the constant torque region is as follows:

$$i_d > i_{d\_\mathrm{MTPA}} \tag{40}$$

Simulations have been performed with an 110 kW IPMSM. Parameters of the IPMSM are shown in Table 1.

Table 1. Parameters of the interior permanent magnetic synchronous motor.

Parameters	Value
DC-link voltage	550 V
Rated speed	3400 rpm
Rated torque	320 Nm
Number of pole pairs	4
Phase resistance	0.2 Ω
d-axis inductance	0.00069 H
q-axis inductance	0.00129 H
Magnet flux linkage	0.1595 Wb

Figure 4 shows the simulation results under step torque changing of CTMPC and PI controller. Both of the output torque of CTMPC and PI controller can track the reference torque very well shown in Figure 4a. The response speed of CTMPC and PI controller is about 0.02 s. Under PI controller, in order to enhance the response speed, the overshoot currents are inevitable shown in Figure 4b, while CTMPC can achieve the same response speed without any overshoot. For a high-power IPMSMs-driven system, in order to increase the power density of the inverter and reduce the cost, the margin of the inverter is limited. With the increase of the working current, the overshoot current under step torque changing may exceed the maximum current which the inverter can bear, and result in the damage of the inverter. Therefore, if the CTMPC proposed in this paper is adopted, the security of driven system will be increased.

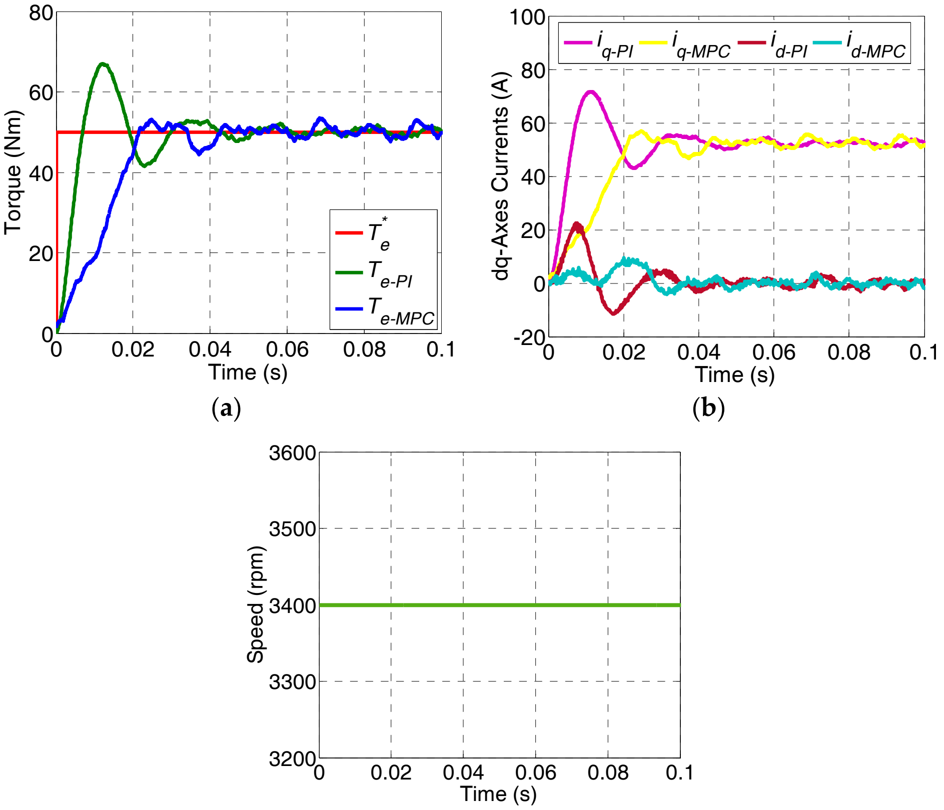

(**a**) (**b**)

(**c**)

Figure 4. Simulation results under the step torque changing of the continuous-time model predictive control and proportional integralcontroller (**a**) Torque; (**b**) dq-Axes Currents; (**c**) Speed.

Besides, for a high-power IPMSMs-driven system, in order to protect the inverter, the maximum values of dv/dt and di/dt should be limited. With those limitations, the response speeds of CTMPC and PI are slower than standard controllers.

Figure 5 is the simulation results under an adjustable DC-link voltage ranging from 270 V to 210 V at 1300 rpm. The reference torque is 35 Nm during simulation. With the decreasing of DC-link voltage, MI is increased as shown in Figure 5d. After 0.4 s, since the MI is equal or bigger than 0.907, the working condition of the motor changes to the FW region from the constant torque region. Then, the demagnetizing current (i_d) is increased significantly with the decreasing of the DC-link voltage shown in Figure 5c. Simultaneously, γ changes from 17.5° to 21.5° (Figure 5e). It should be noted that during simulation, i_q maintains on 36.6 A basically. The simulation results indicate that the proposed CTMPC can ensure the smooth transition between the constant torque region and the FW region under the adjustable DC-link voltage since the output torque can track the reference value very well, as shown in Figure 5b. The simulation results also indicate that the area of FW region is enlarged, owing to the decreasing of DC-link voltage. For a given speed and torque, the operation (constant torque or FW) may be different according to DC-link voltage. Therefore, it is important to determine the transiting point by MI.

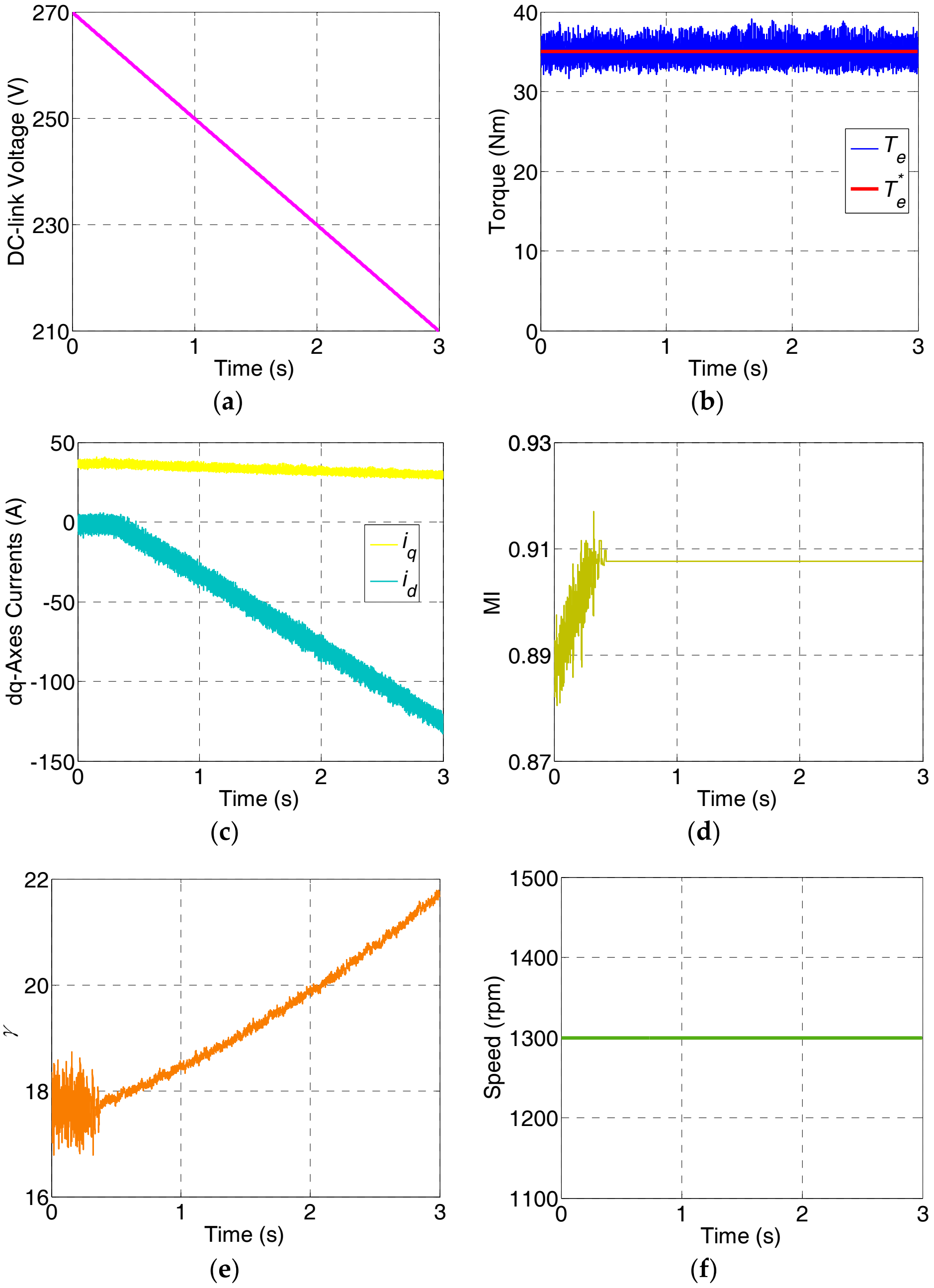

Figure 5. Simulation results under an adjustable DC-link voltage. (**a**) DC-link voltage; (**b**) Torque; (**c**) dq Axes-Currents; (**d**) Modulation Index (MI); (**e**) γ; (**f**) Speed.

Figure 6 shows the simulation results with the IPMSM entering and leaving the FW region with the changing of reference torque. During 0–4 s, the reference torque is 50 Nm. After that, the reference torque increases slowly to 200 Nm at 7 s. Then, the reference torque decreases to 50 Nm at 16 s. During 16–17 s, the reference torque is 50 Nm again. With the increasing of torque shown in Figure 6a, MI (Figure 6c) increases, too. When MI reaches the maximum value 0.907 (about 4 s), the constant torque region changes into the FW region. During 4–7 s, i_d and γ both increase with the increase of the reference torque as shown in Figure 6b,d. After that, i_d and γ both decrease because of the decrease of the output torque. When i_d equals to 0 at about 20 s (Figure 6b), IPMSM leaves the FW region. With the proposed method, the IPMSM can be controlled very well on the FW region. The proposed method can realize the seamless transition between the two modes.

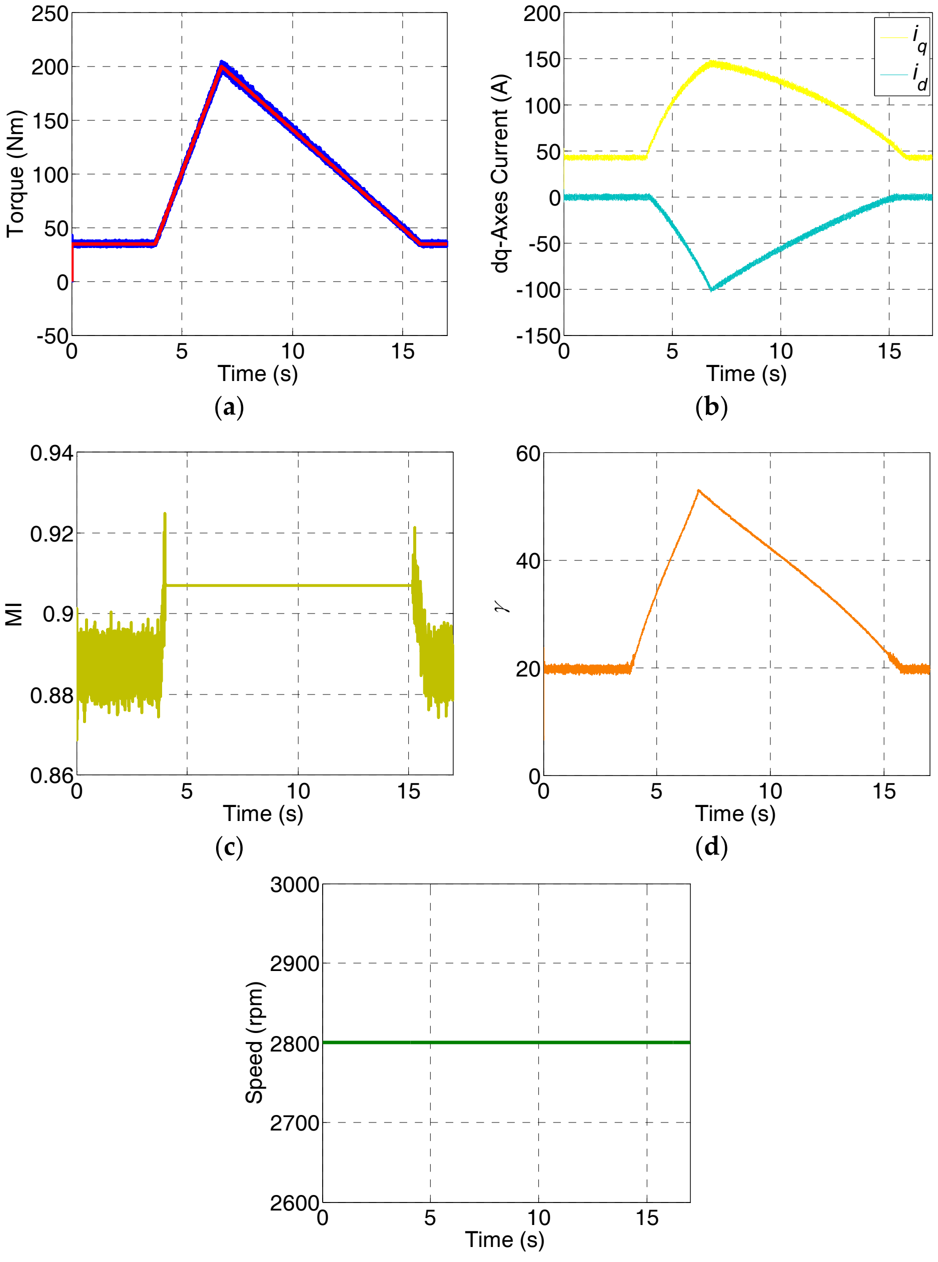

(**a**) (**b**)

(**c**) (**d**)

(**e**)

Figure 6. Simulation results of the transition between the constant torque and the FW region with the output torque changing. (**a**) Torque; (**b**) dq-Axes Currents; (**c**) MI; (**d**) γ; (**e**) Speed.

4. Experiment Results

The experimental setup includes an inverter, an IPMSM, a transmission, and a load shown in Figure 7. The transmission can change the transmission ratio of driven system, and expand its working scope. The load is another IPMSM which works as a generator. It can keep the driven system working at the given speed. A host PC is used to run the user interface (RS-232 connected) and the DSP development and debugger tools (JTAG connected). RS-232 is applied to send instructions to the inverter and receive signals from the inverter. The communication speed of RS-232 is about 0.5 s. The controller area network (CAN) of the DSP is used to collect the signals of control variables and state variables since the communication speed of RS-232 is lower than CAN, such as MI, γ, DC-link voltage, currents, speed, etc. The communication speed of the CAN is 250 kbps.

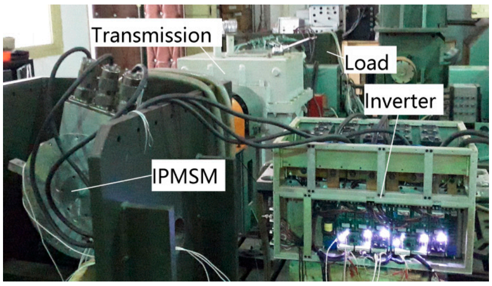

Figure 7. Experimental setup.

Figure 8 shows the experiment results under the step torque changing of CTMPC and PI controller. The reference torque is 50 Nm. Both the output torque of the CTMPC and PI controller can track the reference value accurately. The response speed of CTMPC and PI controller is about 0.02 s. When CTMPC is adopted, the overshoot phenomenon is restrained which is one of the advantages of CTMPC.

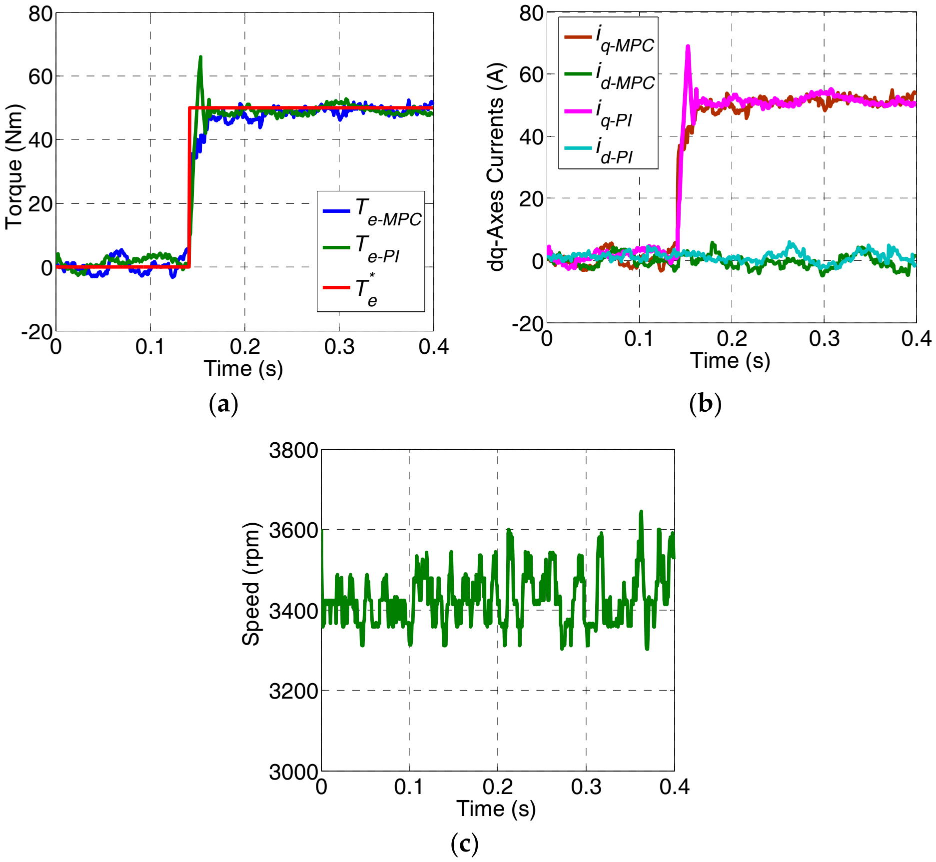

Figure 8. Experiment results under step torque changing of the CTMPC and PI controller. (**a**) Torque; (**b**) dq-Axes Currents; (**c**) Speed.

The simulation and experimental results of proposed CTMPC and PI controller with step torque changing are basically the same. However, constrained by the communication speed of CAN, simulation results can reveal more details than experimental results.

Figure 9 shows the experiment results of proposed CTMPC under the adjustable DC-link voltage. The DC-link voltage is changing from 268 V to 224 V during experiment as shown in Figure 9a. The reference torque is 35 Nm, and the output torque can track the reference value basically shown in Figure 9b. With the decreasing of DC-link voltage, at about 0.4 s, MI is increasing to 0.907. The working state of IPMSM is switching to the FW region from the constant torque region. The experimental results show that the proposed CTMPC can ensure the smooth transition between the constant torque region and FW region under changeable DC-link voltage.

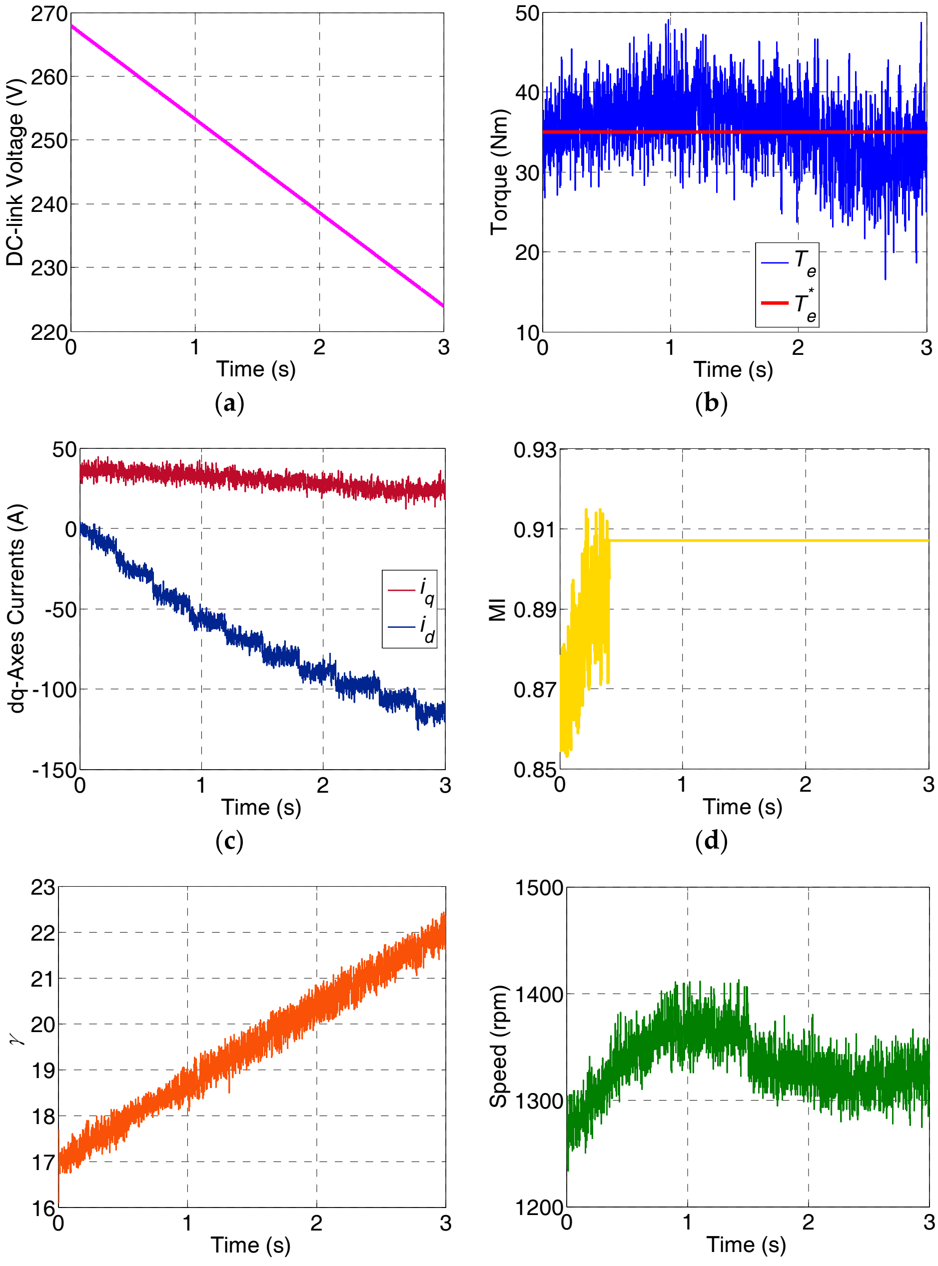

(**a**) (**b**) (**c**) (**d**) (**e**) (**f**)

Figure 9. Experiment results under the adjustable DC-link voltage. (**a**) DC-link voltage; (**b**) Torque; (**c**) dq-Axes Currents; (**d**) MI; (**e**) γ; (**f**) Speed.

During the experiment, the speed of driven system is maintained by the other IPMSM, which works as load. The speed of driven system is 1325 rpm basically shown in Figure 9f. Compared with simulation results under the adjustable DC-link voltage (Figure 5), speed fluctuations are more obvious.

Figure 10 shows the experiment results of the proposed CTMPC during entering and leaving FW region by the changing of the reference torque. During the experiment, the changing of reference torque is the same with simulation. At about 4 s, when MI is reaching to 0.907, the work state of IPMSM is switching to the FW region from the constant region. At about 16 s, when i_d is decreasing to 0, the work state of IPMSM is switching back to the constant region from the FW region. During experiment, the output torque can track the references basically according to Figure 10a. Therefore, the proposed CTMPC can ensure the smooth transition between the constant torque and FW regions under the changing output torque.

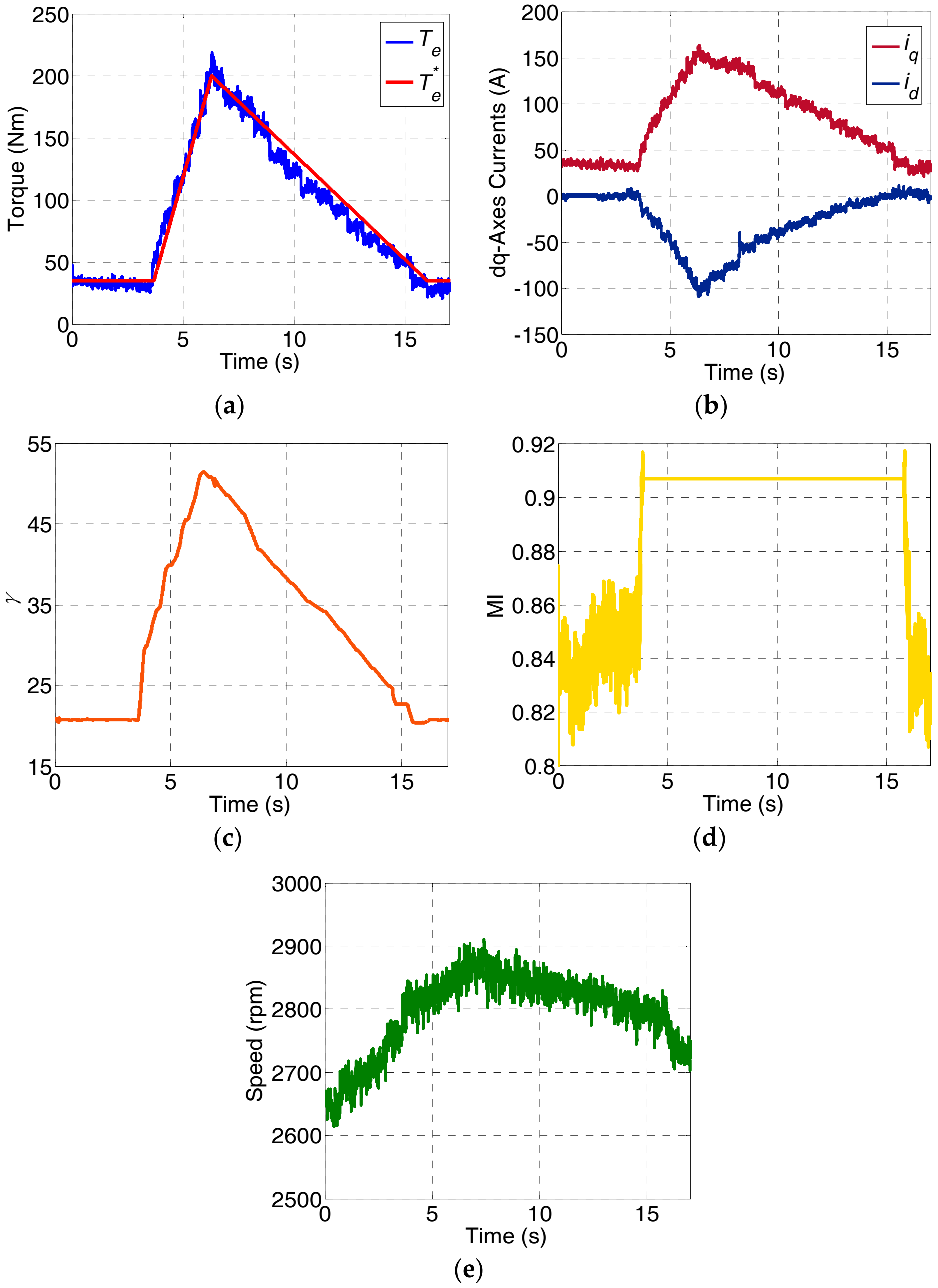

(**a**) (**b**) (**c**) (**d**) (**e**)

Figure 10. The experiment results that the transition of interior permanent magnetic synchronous motor between the constant torque and FW region with the output torque changing. (**a**) Torque; (**b**) dq-Axes Currents; (**c**) γ; (**d**) MI; (**e**) Speed.

5. Conclusions

Two CTMPC models are proposed to describe the properties of PMSMs in the constant torque region and the FW region respectively for the aim of performance improvement. Due to the limitation of the DC-link voltage, the mathematical model of PMSMs in FW region is nonlinear, so the increment of the voltage angle is linearized at each sample time. Therefore, the proposed CTMPC has obvious advantages in dealing with systems non-linear constrains and reducing computation load of DSP. Besides, the proposed CTMPC can restrain the overshoot current with torque step changing, which can enhance the safety of inverter. The selection of transition points between the constant torque region and the FW region is also presented. Both simulation and experimental results show that the proposed CTMPC can ensure the smooth transition between the constant torque and FW regions even under changing DC-link voltage and torque.

Some additional issues will be addressed in the future, including the improving of torque accuracy, the robustness of the controller, and the increasing of the response speed.

Acknowledgments: The work was supported by the National Natural Science Foundation of China (Grant no. 51677005). The authors gratefully acknowledge their support.

Author Contributions: Dandan Su wrote the paper; Chengning Zhang conceived and designed the experiments; Yugang Dong performed the experiments and analyzed the data.

Conflicts of Interest: The authors declare no conflict of interest.

References

1. Saverio, B.; Silverio, B.; Luca, P.; Mauro, Z. Design and implementation of model predictive control for electrical motor drives. *IEEE Trans. Ind. Electron.* **2009**, *56*, 1925–1936.
2. Xiong, R.; Cao, J.Y.; Yu, Q.Q. Reinforcement learning-based real-time power management for hybrid energy storage system in the plug-in hybrid electric vehicle. *Appl. Energy* **2018**, *211*, 538–548. [CrossRef]
3. Lin, C.K.; Yu, J.; Lai, Y.S.; Yu, H.C. Improved model-free predictive current control for synchronous reluctance motor drives. *IEEE Trans. Ind. Electron.* **2016**, *63*, 3942–3953. [CrossRef]
4. Sönke, T.; Nils, H.; Friedrich, W.F. PI control, PI-based state space control, and model-based predictive control for drive systems with elastically coupled loads—A comparative study. *IEEE Trans. Ind. Electron.* **2011**, *58*, 3647–3657.
5. Jorge, R.D.; Antonio, N.; Marco, A.M.; Alexander, G.L.; José, C. Digital sliding-mode sensorless control for surface-mounted PMSM. *IEEE Trans. Ind. Inform.* **2014**, *10*, 137–150.
6. Qiao, Z.W.; Shi, T.N.; Wang, Y.D.; Yan, Y.; Xia, C.L.; He, X.N. New sliding-mode observer for position sensorless control of permanent-magnet synchronous motor. *IEEE Trans. Ind. Electron.* **2013**, *60*, 710–719. [CrossRef]
7. Hicham, C.; Pierre, S. Adaptive fuzzy logic control of permanent magnet synchronous machines with nonlinear friction. *IEEE Trans. Ind. Electron.* **2012**, *59*, 1123–1133.
8. Kim, S.K.; Lee, J.S.; Lee, K.B. Offset-free robust adaptive back-stepping speed control for uncertain permanent magnet synchronous motor. *IEEE Trans. Power Electron.* **2016**, *31*, 7065–7076. [CrossRef]
9. Ahmed, R.; Paul, Y. Hardware/software implementation of fuzzy-neural-network self-learning control methods for brushless DC motor drives. *IEEE Trans. Ind. Electron.* **2016**, *52*, 414–424.
10. Fu, X.G.; Li, S.H. A novel neural network vector control technique for induction motor drive. *IEEE Trans. Energy Convers.* **2015**, *30*, 1428–1437. [CrossRef]
11. Wang, X.G.; Wang, X.Y.; Fu, T.; Wang, J. Predictive instantaneous torque control for disc coreless permanent magnet synchronous motor with the current source chopper. *IEEE Trans. Power Electron.* **2015**, *30*, 7100–7112. [CrossRef]
12. Xiong, R.; Zhang, Y.; He, H.; Zhou, X.; Pecht, M. A double-scale particle-filtering, energy state prediction algorithm for lithium-ion batteries. *IEEE Trans. Ind. Electron.* **2017**. [CrossRef]
13. Xiong, R.; Tian, J.P.; Mu, H.; Wang, C. A systematic model-based degradation behavior recognition and health monitor method of lithium-ion batteries. *Appl. Energy* **2017**, *207*, 372–383. [CrossRef]
14. Zhou, D.H.; Zhao, J.; Liu, Y. Predictive torque control scheme for three-phase four-switch inverter-fed induction motor drives with DC-link voltages offset suppression. *IEEE Trans. Power Electron.* **2015**, *30*, 3309–3318. [CrossRef]
15. Wang, F.; Li, S.; Mei, X.; Xie, W.; Rodríguez, J.; Kennel, R.M. Model-based predictive direct control strategies for electrical drives: An experimental evaluation of PTC and PCC methods. *IEEE Trans. Ind. Electron.* **2015**, *11*, 671–681. [CrossRef]

16. Chen, C.; Xiong, R.; Shen, W. A lithium-ion battery-in-the-loop approach to test and validate multi-scale dual H infinity filters for state of charge and capacity estimation. *IEEE Trans. Power Electron.* **2018**, *33*, 332–342. [CrossRef]
17. Yu, Q.Q.; Xiong, R.; Lin, C.; Shen, W.X.; Deng, J.J. Lithium-ion Battery Parameters and State-of-Charge Joint Estimation Based on H infinity and Unscented Kalman Filters. *IEEE Trans. Veh. Technol.* **2017**, *66*, 8693–8701. [CrossRef]
18. Xiong, R.; Yu, Q.Q.; Wang, L.Y.; Lin, C. A novel method to obtain the open circuit voltage for the state of charge of lithium-ion batteries in electric vehicles by using H infinity filter. *Appl. Energy* **2017**, *207*, 346–353. [CrossRef]
19. Chen, Y.; Liu, T.H.; Hsiao, C.F.; Lin, C.K. Implementation of adaptive inverse controller for an interior permanent magnet synchronous motor adjustable speed drive system based on predictive current control. *IET Electr. Power Appl.* **2015**, *9*, 60–70. [CrossRef]
20. Zhang, X.G.; Hu, B.S.; Mei, Y. Deadbeat predictive current control of permanent magnet synchronous motors with stator current and disturbance observer. *IEEE Trans. Power Electron.* **2016**, *18*, 31–41. [CrossRef]
21. Xin, L.; Pourya, S. Model predictive current control of switched reluctance motors with inductance auto-calibration. *IEEE Trans. Ind. Electron.* **2016**, *63*, 3934–3941.
22. Alexandros, D.A.; Nikolaos, K.; Adamopoulos, A. Development of a constant switching frequency deadbeat predictive control technique for field-oriented synchronous permanent-magnet motor drive. *IEEE Trans. Ind. Eletron.* **2016**, *63*, 5167–5175. [CrossRef]
23. Hao, Z.; Xi, X.; Li, Y.D. Torque ripple reduction of the torque predictive control scheme for permanent-magnet synchronous motors. *IEEE Trans. Ind. Electron.* **2012**, *59*, 871–877.
24. Cho, Y.; Lee, K.B.; Song, J.H.; Lee, Y.I. Torque-ripple minimization and fast dynamic scheme for torque predictive control of permanent-magnet synchronous motors. *IEEE Trans. Power Electron.* **2015**, *30*, 2182–2190. [CrossRef]
25. Xia, C.L.; Qiu, X.D.; Wang, Z.Q.; Shi, T.N. Predictive torque control for voltage source inverter-permanent magnet synchronous motor based on equal torque effect. *IET Electr. Power Appl.* **2016**, *10*, 208–216. [CrossRef]
26. Zhang, Y.C.; Yang, H.T.; Xia, B. Model predictive torque control of induction motor drives with reduced torque ripple. *IET Electr. Power Appl.* **2015**, *9*, 595–604. [CrossRef]
27. Habibullah, M.; Lu, D.D.; Xiao, D.; Rahman, M.F. A simplified finite-state predictive direct torque control for induction motor drive. *IEEE Trans. Ind. Electron.* **2016**, *63*, 3964–3975. [CrossRef]
28. Linder, A.; Kennel, R.; Linke, M. Generalized predictive control (GPC)-Ready for use in drive applications? In Proceedings of the 32nd IEEE Annual Power Electronics Specialists Conference (PESC), Vancouver, BC, Canada, 17–21 June 2001; pp. 1839–1844.
29. Su, D.D.; Zhang, C.N.; Dong, Y.G. An improved generalized model predictive control for permanent magnetic synchronous motors for wide-speed range. In Proceedings of the ISEV 2017, Stockholm, Sweden, 26–29 July 2017.
30. Patxi, A.; Oscar, B.; José, A.C.; Asier, Z. Efficient multivariable generalized predictive control for sensorless induction motor drives. *IEEE Trans. Ind. Electron.* **2014**, *61*, 5126–5134.
31. Eudemario, S.S.; Edson, B.; Wagner, C.A. A Predictive Algorithm for Controlling Speed and Rotor Flux of Induction Motor. *IEEE Trans. Ind. Electron.* **2008**, *55*, 4398–4407.
32. Rachid, E.; Ahmed, A.D.; Muyeen, S.M.; Leng, S.Y. Continuous-time model predictive control of a permanent magnet synchronous motor drive with disturbance decoupling. *IET Electr. Power Appl.* **2017**, *11*, 697–706.
33. Rachid, E.; Muyeen, S.M.; Ahmed, A.D. Experimental Validation of a Robust Continuous Nonlinear Model Predictive Control Based Grid-Interlinked Photovoltaic Inverter. *IEEE Trans. Ind. Electron.* **2016**, *63*, 4495–4505.